Assessment of Half-decadal variability of Mangrove health cover over the Indian Sundarban region using Remote Sensing and GIS technique.

Abstract:

The present study aims to assess changes of mangrove vegetation with their cause and impact over a period of 30 years, from 1990 to 2019. The density of mangrove variability in half decadal level was calculated based on Normalized Differential Vegetation Index (NDVI) composites derived using 30m spatial resolution temporal Landsat Thematic Mapper (TM) & Operational Land Imager (OLI) data pertaining to Indian part of Sundarban Mangrove Forest. Further, variability of Half Decadal Change of Mangrove Density (HDCMD) was calculated using the consecutive NDVI composites. The results of HDCMD have shown large spatio-temporal variability, maximum HDCMD recorded during 1995, 2000 & 2014 with strong positive correlation (0.85) with Net Rainfall Change (NRC) and negative correlation (-0.82) with bio-carbon flux. The dense and healthy mangroves contribute in sinking bio-carbon from atmosphere, acting as good source sink. A net change in the HDCMD reveals overall improvement in the mangrove cover during 1989-2019. However, the threat of coastal erosion on mangrove environ along the southern sea fronts persists. Besides, the mangrove cover increased in prevailing depositional environments of islands and banks of creeks. The outcomes of such study are useful in sustainable coastal zone management, planning, environment and climate change.

Keywords: Mangroves, shoreline change, Rainfall, Landsat, Bio-carbon flux, NDVI

Introduction

Mangroves are highly productive coastal wetlands supporting rich biodiversity and occurring mainly in tropical and subtropical regions under specific salinity and temperature conditions. The Sundarbans, the world's largest continuous mangrove forest shared by India and Bangladesh, lie on the delta of the Ganges, Hooghly, Padma, and Brahmaputra rivers and are internationally recognized as both a UNESCO World Heritage Site (1987) and a Ramsar wetland (2019), yet

remain increasingly threatened by human activities and climate change. Currently, mangrove covers 4921 $km^{2,}$ which has shown a modest increment in the cover from 1987(4,046 km^2) to the current status. Giri et. al., (2011) state that the mangroves that once extended along the 7516.6 km long coastline of the Indian counterpart have been constantly reducing. Data from the Forest Survey of India indicate that mangrove area in the Indian Sundarbans increased between 1987 and 2017 based on satellite observations. In the past 3 decades, marginally 0.061% per year has increased in the Sundarbans. However, the spatio-temporal variability of mangrove is changing year by year due to sea level rise [1] and changes in the fresh water flows from Himalayan rivers which are among the major disturbances threatening these coastal areas. Variation in precipitation will have an impact on the mangrove density and health. It has been demonstrated in earlier studies that increased precipitation helps expand mangrove cover [2] and improve species richness and diversity due to decreased salinity [3]. It is quite obvious that the dynamic coastal environ such as Sundarban, will have an impact on mangrove cover due to erosion and accretion [4,5].

The increase in atmospheric CO_2 is a key driver of climate change, with concentrations rising by nearly 40% since pre-industrial times. This rise, primarily caused by fossil fuel use and bio-flux processes such as deforestation and drought, underscores the importance of studying year-to-year variability in mangrove carbon sources and sinks [6–8].

Forests act as carbon sinks or sources by absorbing CO_2 through photosynthesis and releasing it during respiration, with carbon stored in biomass and soils. Mangroves are exceptional carbon reservoirs, storing 956 Mg C ha^{-1}far exceeding most terrestrial forests and their high productivity aids climate change mitigation, with carbon fluxes commonly assessed using field measurements and remote sensing approaches [9,10].

Variations in mangrove vegetation across space and time play a crucial role in carbon cycle studies, with NDVI widely applied to quantify green biomass and canopy photosynthetic activity. Besides, NDVI is also most widely used in the context of ecosystem studies because it was shown to be closely related to biomass and intensity of photosynthesis, respiration, net primary productivity, net CO2 exchange, etc [11,12].

The red and near-infrared bands of Landsat imagery were employed to compute NDVI.This is well established technique to extract the vegetation classes. Healthy vegetation will absorb most of the lights in visible red spectrum reflecting a large portion of the near-infrared light [13-17]. Contrary to this, unhealthy or sparse vegetation reflect more in red light and less in near-infrared spectrum which can distinguish degree of sparse/dense mangrove vegetation with high accuracy [18].

Few studies have attempted on the carbon estimation using the *in situ* observations in the Sundarban Mangrove Forest area. Hence current study is an attempt to use the remote sensing technique to assess the long-term spatio-temporal NDVI changes to decipher the health of mangrove and further inter-relate with the bio-carbon flux in the Sundarban Mangrove Forest environment [19-22]. The study aims to quantify half-decadal variability in mangrove density using NDVI data from 1990–2019 and to estimate mangrove cover changes driven by rainfall intensity and shoreline dynamics affecting bio-carbon flux.

Study Area

The Indian Sundarbans, situated on the Gangetic delta along the West Bengal coast, represent the world's largest mangrove wetland with high sedimentation rates. Located between 21°33′–22°12′ N and 88°16′–89°05′ E, the area experiences a subtropical monsoon climate with heavy rainfall and recurrent cyclonic activity.

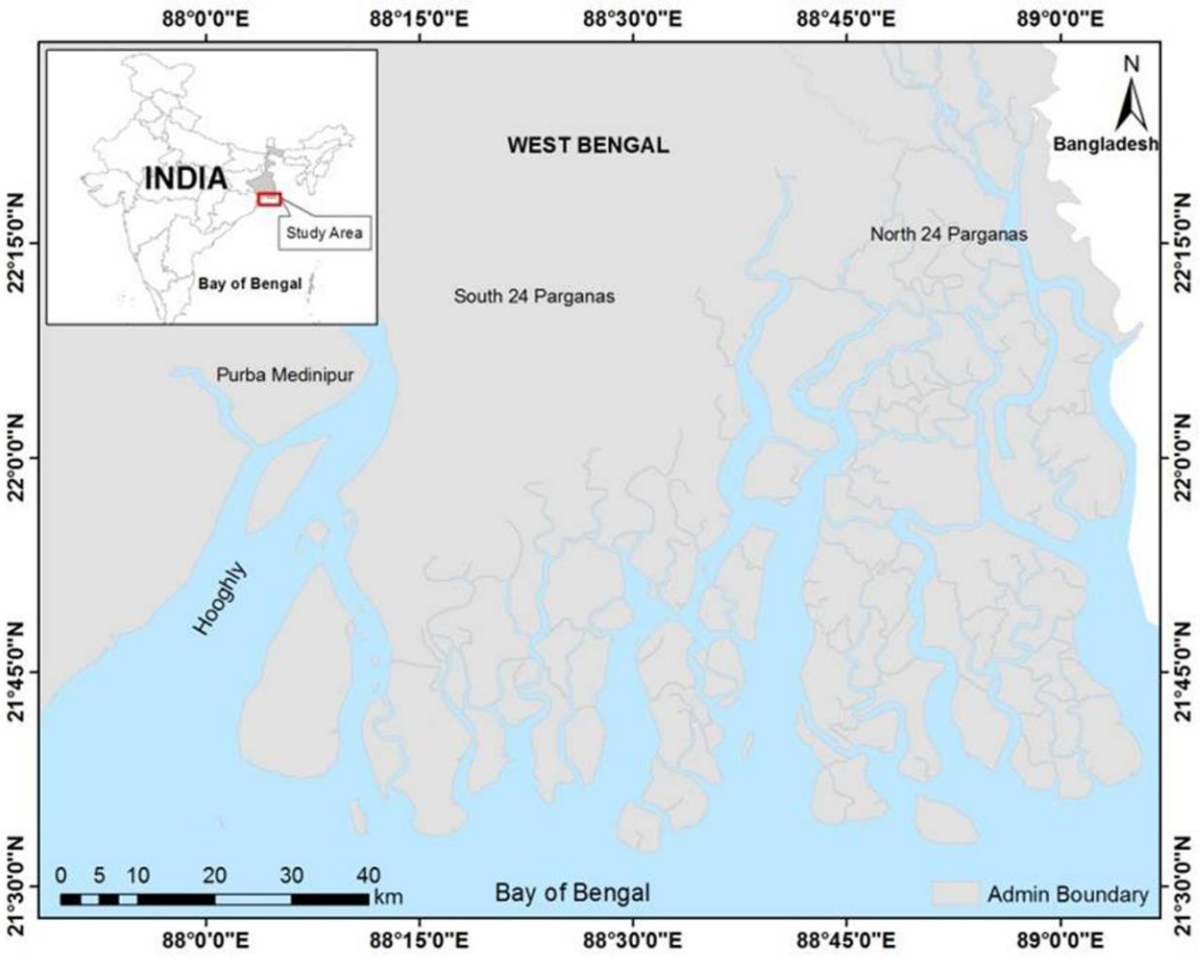

Figure 1: Showing the Study Area

Data and Methods

This study employed multi-date Landsat data from USGS, including TM and OLI sensors (Table 1). Images were carefully selected to ensure comparable seasonal and tidal conditions [23,24]. Mangrove areas were identified using tone and colour contrast in FCC (5–4–3) images, and DN values were transformed into reflectance after atmospheric correction.

$$P_\lambda = M\lambda Q_{cal} + A_\lambda \text{----------} 1$$

where, P_λ = Planetary reflectance without correction for sun angle, M_λ = Reflectance multi band, A_λ = Reflectance add band, Q_{cal} = Digital number.

Table1: Landsat datasets used in the present study

Satellite data	Sensor	Date of acquisition	Spatial Resolution in m	Path/Row
LANDSAT 5	TM	1990-01-14	30	138/45
LANDSAT 5	TM	1995-01-28	30	138/45
LANDSAT 5	TM	2000-01-26	30	138/45
LANDSAT 5	TM	2005-01-07	30	138/45
LANDSAT 5	TM	2010-01-21	30	138/45
LANDSAT 8	OLI TIRS	2014-12-18	30	138/45
LANDSAT 8	OLI TIRS	2019-01-30	30	138/45

The atmospheric correction (AC) has been applied to all the datasets using ACOLITE is coded in Python 3. It includes "Dark Spectrum Fitting" (DSF) algorithm for atmospheric correction.

The Dark Spectrum Fitting (DSF) algorithm estimates atmospheric path reflectance (ρpath) by assuming spatially uniform atmospheric conditions and the presence of dark pixels with near-zero surface reflectance within the scene. A dark spectrum is derived from minimum observed top-of-atmosphere reflectance values, and radiative transfer modeling is used to simulate ρpath for multiple aerosol types and aerosol optical thickness (τa) values. The lowest non-zero τa is selected to avoid negative surface reflectance, and the optimal aerosol model is identified by minimizing the root mean squared difference between observed and modeled reflectance. Atmospheric correction separates atmospheric and surface signals, after which red and near-infrared surface reflectance bands from Landsat-5 TM and Landsat-8 OLI were used to compute NDVI.

The surface reflectance of Red & Infra-Red bands were used for NDVI classification using band ratio (IR-R) with (IR+R) in equation (1) on each images pertaining all bi-decadal data set. These NDVI indices values have range between -1 to 1 and positive values obtained represent

mangroves with different density levels (since the image fed into NDVI calculation consist only mangrove area).

$$\textbf{NDVI} = \frac{(IR-R)}{(IR+R)} \text{--------} (1)$$

The running HDCMD was calculated by subtracting from later image to earlier image. Example, the HDCMD in between 1995 to 2000 was calculate by subtracting 1995 NDVI (later) from 2000 NDVI (earlier) imagery. Hence positive values in HDCMD indicate increase in mangrove density and negative value indicate decrease. Similarly, the running HDCMD was calculated for every five year intervals during 1990-2019 i.e., 1990-95, 1995-2000, 2000-2005, 2005-2010, 2010-2014 and 2014-2019. Besides, the HDCMD was also calculated for net period during 1990-2019. Level of improvement, degradation and no change was estimated based on the HDCMD values defined in the Table 2.

Table 2. Criteria for the classification of different mangrove change classes based on HDCMD values and their indexes

Mangrove Change	HDCMD	
	Values Range	**Index**
Loss	< -1	-5
Densely Loss	-0.5 to -1	-4
Sparsely Loss	<0 to -0.5	-2
No Change	0	0
Sparsely Gain	> 0 to 0.5	2
Densely Gain	0.5 to 1	4
Gain	> 1	5

Finally the area of HDCMD at each period were calculated and classified into 5 classes index applying different conditions: (1) if NDVI value of 2nd (later) image is greater than 0 but 1st (earlier) image is less than 0 then it is assigned as -5 (Mangrove/Erosions Lost completely), (2) if difference value is >= -2.785 & < -0.027 then assigned as -4 (Degradation Mangrove); (3) if

difference value is >= -0.027 & < 0.039 then assigned as 0 (small change/No change Mangrove);(4) if difference value is >= 0.039 and <= 2.75 as 4 (Improve Mangrove); (5) if 2nd image is greater than 0 but 1st image is less than 0 is assigned to +5 (new mangrove/Accretion). The further maps and statistics for each period were generated based on above HDCMD classification.

In this study the monthly 0.25 X 0.25 degree gridded TRMM rainfall data during 1997 to 2017 pertaining to study area was used to estimate the variation and their impact on Mangrove density. The average rainfall of preceding season (6 months) from the month of each Landsat data was used. This is one among other parameters which helps in maintaining the health of mangroves. The change in the average rainfall between two consecutive periods were estimated to correlate with mangrove changes. The average rainfall of preceding season pertaining to two consecutive period was subtracted (earlier minus later) to calculate Net Rainfall Change (NRC). Further, relation between NRC and HDCMD were established at each period.

Bio-carbon flux corresponding to each HDCMD phase was derived from monthly CarbonTracker data at one-degree resolution for 2000–2018. NBCF was estimated by subtracting earlier flux values from later ones, where negative NBCF denotes carbon sequestration linked to mangrove expansion and positive NBCF indicates mangrove decline. The relationship between NBCF and HDCMD was evaluated to understand mangrove carbon dynamics. Shoreline change rates were calculated from multi-temporal Landsat imagery using digitized shorelines and DSAS-based EPR statistics to identify zones of erosion and accretion affecting mangrove cover.

Monthly bio-carbon flux with respect to each HDCMD period (month of Landsat data acquired) were extracted from one-degree monthly NOAA carbon flux tracker data (ftp://aftp.cmdl.noaa.gov/products/carbontracker/co2/fluxes/monthly/) during 2000 to 2018 period based on availability. The Net Bio-Carbon Flux (NBCF) pertaining to the consecutive period was estimated by subtracting bio-carbon flux of earlier with later periods. The negative value of NBCF indicates the sink of carbon by biosphere (mangrove) due to an increase in the mangrove density. In contrast, positive value of NBCF indicates a decrease in mangrove density. The current study is an effort to establish a relation between NBCF and HDCMD to understand the role (source/sink) of mangrove density on bio-carbon flux [25-28].

Results and Discussions

The Figure 2 shows composites of HDCMD calculated during period 1990 & 1995 (a), 1995 &2000 (b), 2000 & 2005 (c), 2005 & 2010 (d), 2010 & 2014 (e) and 2014 & 2019 (f). Notable increase in the HDCMD was observed from 1995 to 2000 by densely gaining 2201.3 km^2 whereas, 63.9 km^2 area has been sparsely lost in the south western parts and 15.4 km^2 of the mangroves completely lost (red color shown on legend) along the seaward side of the islands. But an increase (newly grown mangroves) of 71.8 km^2 area could be seen on several parts of the islands in the estuaries/creeks. This may be due to change in the marine-fluvial process that favor mangrove growth in these small island environs. On the other hand, NRC increase up to 25.11 mm/day was recorded during 1995-2000 (Figure 4), which is significantly higher than an average. This increase in rainfall was attributed to the dense growth of mangrove trees during 1995-2000.

The HDCMD between 2000 and 2005 decreased considerably as shown in Figure 2c. A total of 2163.8 km^2 area shown marginal loss in the mangrove vegetation, whereas for 44.3 km^2 area the mangrove cover was completely lost. During the same period on the other hand, 129.1 km^2 area shown significant gain in the mangrove density while only for 6.3 km^2 area the new mangrove cover was recorded. The complete loss of mangroves on the seaward side continued further in this period as well. We infer that the decrease in the NRC (16.34 mm/days (Figure 4)) during this period could have hurt mangroves, resulting in the observed degradation.

The HDCMD shows increment in the mangroves in between 2005 & 2010 shown in Figure 2d . A total area of 1316.5 km^2 mangroves has been densely gained in the central and western parts of the study area and 27.9 km^2 area has been completely gained. On the other hand, 957.1 km^2 area of mangroves were sparsely lost in the eastern parts and 21.2 km^2 area of mangroves were completely lost. The NRC has slightly increased by 2.12 mm/day (Figure 4) during this period might have resulted in the moderate increase in the mangrove cover. Besides, rate of bio-carbon sink was 0.5179 $gm/m^2/day$ (Figure 5) which indicates moderately healthy vegetation in this period.

The HDCMD has further increased from 2010 to 2014 with a significant growth of mangroves as shown in Figure 2e. An area of 2245 km^2 shows densely gained and 14.60 km^2 area of

183 mangroves. Whereas, 29.4 km^2 areas show sparsely loss and 21 km^2 area of mangroves have
184 been completely lost in the seaward side of islands. NRC further increased by 2.1 mm/days
185 (Figure 4) leads to increase the mangrove cover with a supporting indication of the rate bio-
186 carbon sinking was 0.9047 gm/m^2/day (Figure 5).

187 The HDCMD shows a decreasing pattern during 2014 to 2019 as shown in Figure 2f. Total area
188 of 1705.47 km^2 show sparsely loss of mangroves and 9.2 km^2 mangrove areas were continued to
189 lose completely along the seaward side coasts of islands whereas, 568.9 km^2 area shows densely
190 gain and 45.5 km^2 show completely gained mangroves. The NRC has decreased by 9.86 mm/day
191 (Figure 4) resulting in decrease of mangrove cover. This was indicated by increase in the bio-
192 carbon flux 0.1365 gm/m^2/day (Figure 5) from terrestrial biosphere to atmosphere during this
193 period.

194 Figure 2 Composites of half decadal spatial distribution of Mangrove during 1990 to 2019

195 Net shoreline change rate is overlaid on HDCMD of pertaining to period 1989-2019 as shown in
196 Figure 3. It was observed that the mangroves were continuously lost completely throughout the
197 study period due to coastal erosion along the seaward side of the islands. It was observed that the
198 rate of erosion was more than 20 m/y. It was also observed that, the HDCMD increased
199 significantly during this period by the increase of 2174 km^2 in densely gain class and a total
200 106.8 km^2 area was completely gained. These areas are the islands and banks of the
201 creeks/estuary.

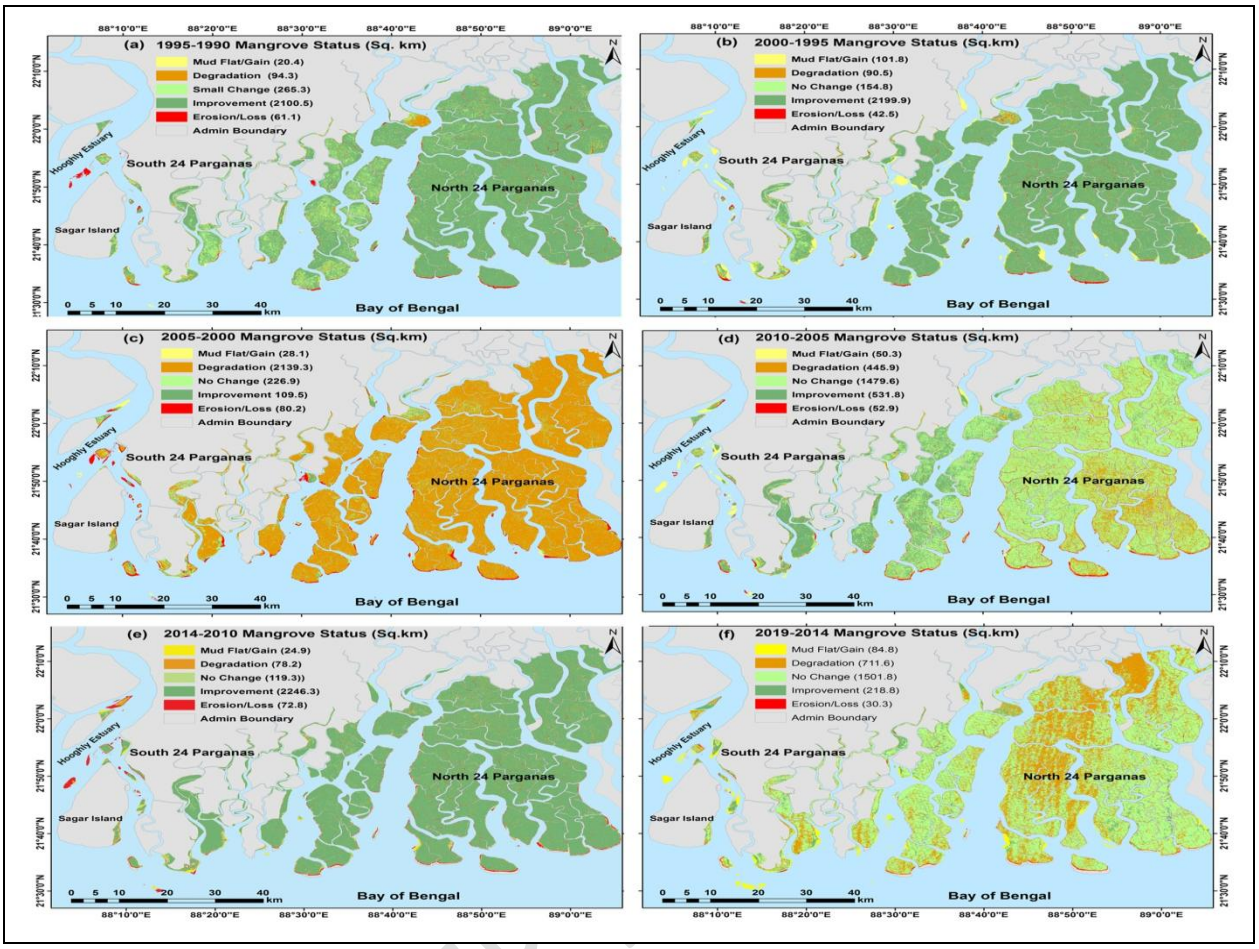

Figure 2: Map showing the composite of HDCMD of 1989-2019 is overlaid with net shoreline change rate

Box-and-whisker plots were used to summarize NDVI variability and inter-period changes throughout the study (Figure 3a, b). The plots present vegetation health along a 0–1 NDVI scale, with quartiles enclosed in the box, whiskers marking data extremes, and outliers shown as individual points beyond the whiskers.

The average NDVI value 0.53+-0.14 (Mean+-SD) with half decadal increasing trend NDVI value 0.03 was observed during study period. The overall period of NDVI value 0.5 to 0.4 under 1st quantile, 0.4 to 0.6 under 2nd quantile, 0.6 to 0.7 under 3rd quantile and 0.7 to 0.95 under 4th quntile. In figure 3b showing the box (2nd to 3rd quantile) bellow '0' said to be degreded period of mangrove and above '0' is said to be improve period of the mangrove. In histogram plot in figure 4 also showing the positive and negative value at the each running half decadal net change of NDVI. From figure 3b & 4 depicting health of Mangroves (vegetation biomass) improved

during 1995, 2000 and 2014. whereas 2005 showing the degraded and 2010 & 2019 showing the no change/small change of mangrove comparative previous half decadal period. This clearly indicating the 2005 and 2010 are the El nino period which effect on the green biomass of the mangrove.

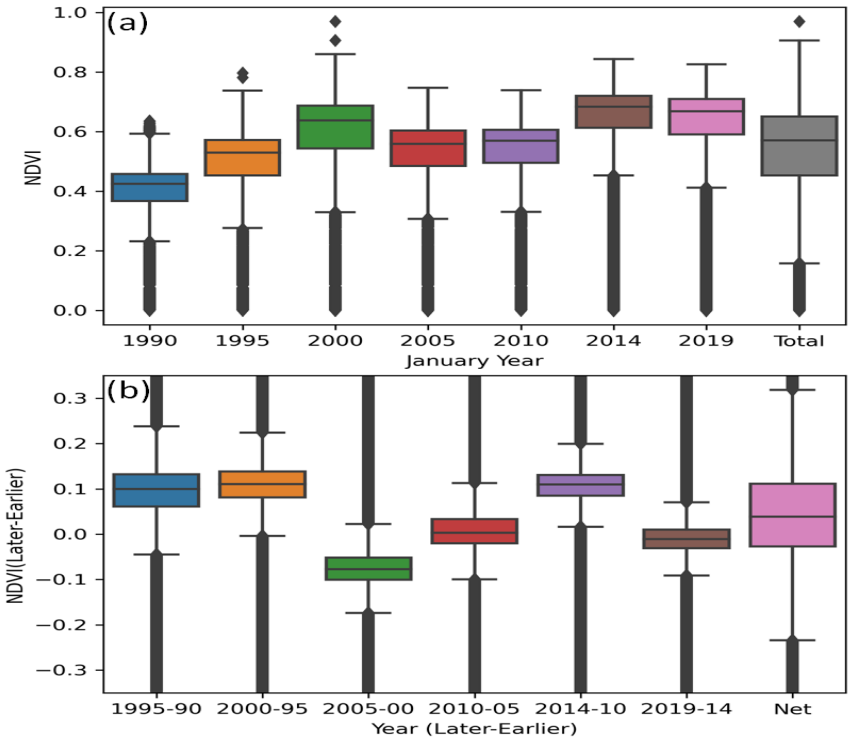

Figure 3: whiskers chart shows interquartile range and the mean of the (a) NDVI and (b) difference of preceding and succeeding NDVI at individual and overall study period

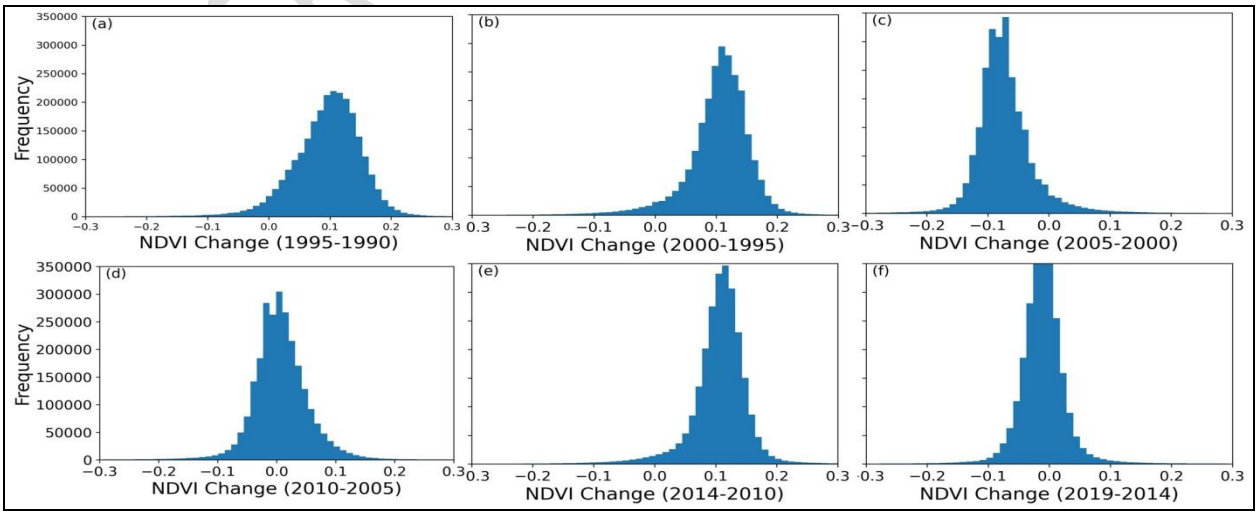

Figure-4: Half decade change of NDVI (Later-Earlier) Histogram during 1990 to 2019

The Figure 5 depicts the relationship between net spatial change of HDCMD and NRC to assess the impact of lead period of rainfall on health of mangrove. It is observed the significant agreement between increase of healthily vegetation by rising NRC with highly positive correlation coefficient of 0.85. In addition to this the variability of sink and source of bio-carbon flux from/to atmosphere was assessed with variation of mangrove cover density. The Figure 6 shows the inter relation between bio-carbon flux with net spatial change of HDCMD. It is observed that, there is significantly agreement of bio-carbon flux with negative correlation (-0.82). It means the net increase of mangrove vegetation contribute to sink carbon from atmosphere or vice versa.

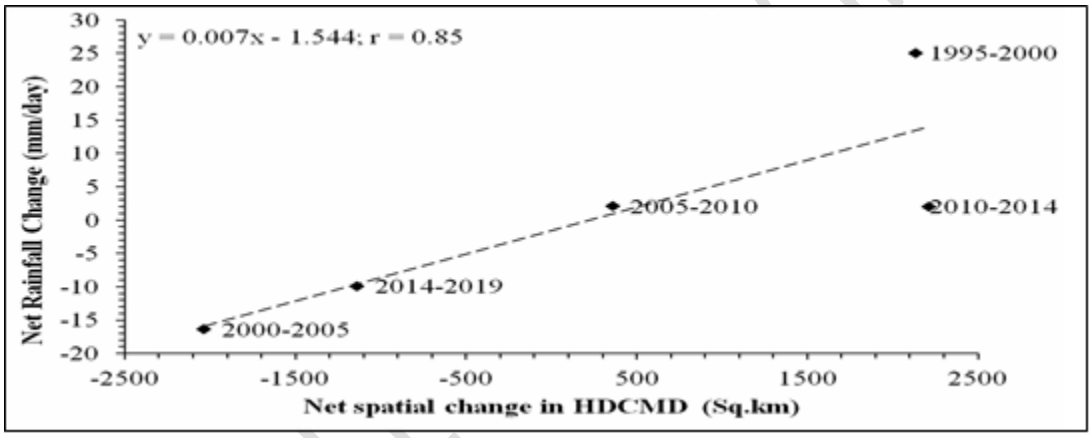

Figure 5 Plot showing the relation between net rainfall change and net spatial change in HDCMD

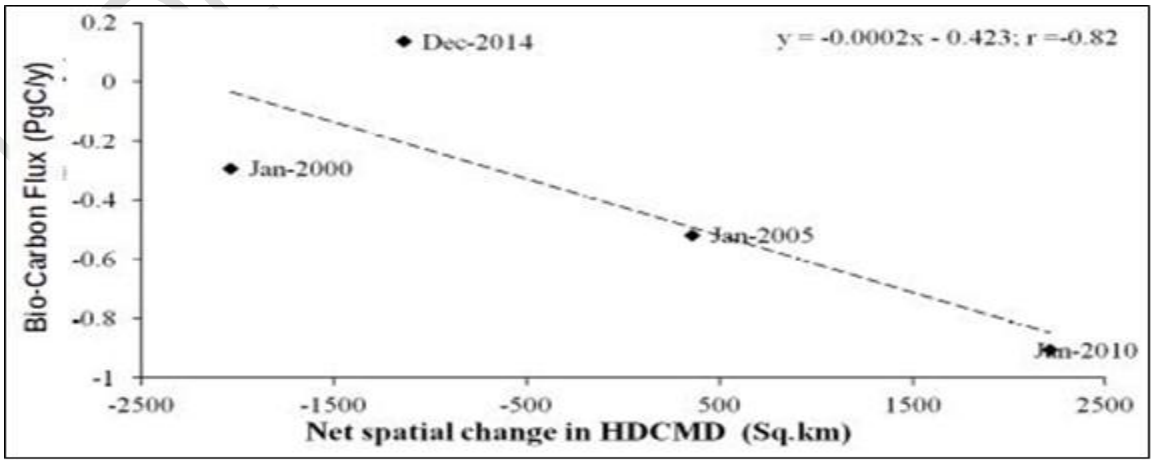

Figure 6 Plot showing the relation between bio-carbon flux and net spatial change in HDCMD

Conclusion

The current study aims at estimating the spatio-temporal changes in the mangrove cover in Indian part of the Sundarbans. It can be inferred that the delineation of mangrove and non-mangrove areas and also classification of HDCMD based on NDVI values is best achieved with help of temporal Landsat imageries. The results also reveal that there is a significant correlation (coefficient 0.85) between HDCMD and NRC. In addition to this, variations in the sink and source of bio-carbon flux at different periods is triggered by health of mangrove vegetation. The study reflects that; there is significant agreement of bio-carbon flux with negative correlation (-0.82) with HDCMD. It indicates the net increase of mangrove density contributes in sinking bio-carbon from atmosphere or vice versa. Good dense mangrove cover (healthy) was observed during 1995, 2000 and 2014 with an increased NRC and good bio-carbon sink. The study concludes the overall improvement in the mangrove cover during 1989-2019. However, the mangroves continue to reduce in the seaward side (southern parts) of eroding islands. On the other hand, the mangroves were picked up in the accretional islands and banks situated inside the estuary/creeks.This knowledge can be used to facilitate suitable planning, management, and regulation of mangrove ecosystems which can be further associated with anthropology and biodiversity to monitor/quantify bio-carbon flux and their consequence on socio-economics of the country.

Acknowledgements

The authors would like to thank USGS for making Landsat data available in open domain, NOAA for carbon tracker data and TRMM for precipitation data.

References

1. Rahman AF, Dragoni D, El-Masri B. Response of the Sundarbans coastline to sea level rise and decreased sediment flow: a remote sensing assessment. Remote Sens Environ. 2011;115:3121–3128. doi:10.1016/j.rse.2011.06.019.

2. Eslami-Andargoli L, Dale P, Sipe N, Chaseling J. Mangrove expansion and rainfall patterns in Moreton Bay, Southeast Queensland, Australia. Estuar Coast Shelf Sci. 2009;85:292–298.

3. Buckney RT. Three decades of habitat change: Kooragang Island, New South Wales. In: Conservation: the role of remnants of native vegetation. Sydney (Australia): Beatty; 1987.

4. Hong PN. Mangroves of Vietnam. Gland (Switzerland): International Union for Conservation of Nature and Natural Resources (IUCN); 1993.

5. Salam M, Lindsay RG, Beveridge C. The use of GIS and remote sensing techniques to classify the Sundarbans mangrove vegetation, Bangladesh. J Agrofor Environ. 2007;1(1):7–15.

6. Thomas JV, Arunachalam A, Jaiswal RK, Diwakar PG, Kiran B. Dynamic land use and coastline changes in active estuarine regions: a study of Sundarban Delta. Int Arch Photogramm Remote Sens Spatial Inf Sci. 2014; XL-8:133–139. doi:10.5194/isprsarchives-XL-8-133-2014.

7. TRMM TMI Rainfall Dataset [Internet]. Honolulu (HI): APDRC, SOEST, University of Hawaii; [cited 2026 Jan 10]. Available from: http://apdrc.soest.hawaii.edu/las/v6/dataset?catitem=13279

8. Nayak RK, Patel NR, Dadhwal VK. Estimation and analysis of terrestrial net primary productivity over India using a remote-sensing-driven terrestrial biosphere model. Environ Monit Assess. 2009. doi:10.1007/s10661-009-1226-9.

9. Knorr W, Heimann M. Impact of drought stress and other factors on seasonal land biosphere CO_2 exchange studied through an atmospheric tracer transport model. Tellus B. 1995;47:471–489.

10. Gitelson AA. Wide dynamic range vegetation index for remote quantification of biophysical characteristics of vegetation. J Plant Physiol. 2004;161(2):165–173.

11. Gonzalez del Castillo E, Sanchez-Azofeifa A, Tha Paw U K, Gamon JA, Quesada M. Integrating proximal broadband vegetation indices and carbon fluxes to model gross primary productivity in a tropical dry forest. Environ Res Lett. 2018;13:065017. doi:10.1088/1748-9326/aac3f0.

12. Bartlett DS, Whiting GJ, Hartman JM. Use of vegetation indices to estimate intercepted solar radiation and net carbon dioxide exchange of a grass canopy. Remote Sens Environ. 1989;30(2):115–128.

13. Guha S. Capability of NDVI technique in detecting mangrove vegetation. Int J Adv Biol Res. 2016;6(2):253–258.

14. Ellison J. How South Pacific mangroves may respond to predicted climate change and sea level rise. In: Climate change in the South Pacific: impacts and responses in Australia, New Zealand, and small island states. Dordrecht: Kluwer Academic; 2000.

15. Field CD. Impacts of expected climate change on mangroves. Hydrobiologia. 1995;295:75–81. doi:10.1007/BF00029113.

16. Giri C, Muhlhausen J. Mangrove forest distributions and dynamics in Madagascar (1975–2005). Sensors. 2008;8(4):2104–2117. doi:10.3390/s8042104.

17. Islam M, Wahab M. A review on the present status and management of mangrove wetland habitat resources in Bangladesh with emphasis on mangrove fisheries and aquaculture. Hydrobiologia. 2005;542:165–190. doi:10.1007/s10750-004-0756-y.

18. Kathiresan K. Mangrove forests of India. Curr Sci. 2018;114(5):976–981. doi:10.18520/cs/v114/i05/976-981.

19. Kumar ST, Mahendra RS, Nayak S, Radhakrishnan K, Sahu KC. Coastal vulnerability assessment for Orissa state, east coast of India. J Coast Res. 2010;26(3):523–534.

20. Mohanty PC, Mahendra RS, Nayak RK, Srinivasa Kumar T. Impact of sea level rise and coastal slope on shoreline change along the Indian coast. Nat Hazards. 2017.

21. Pagkalinawan H. Mangrove forest mapping using Landsat 8 images. In: *Mangrove Proceedings*. 2015;7:60–64.

22. Thieler ER, Danforth WW. Historical shoreline mapping (1): improving techniques and reducing positioning errors. J Coast Res. 1994;10:549–563.

23. Zafar TB, Khan MG. A geographical overview of Sundarban: the largest mangrove forest of Bangladesh. Int J Geol Agric Environ Sci. 2018;6(2):9–10.

24. Bartlett DS, Whiting GJ, Hartman JM. Use of vegetation indices to estimate intercepted solar radiation and net carbon dioxide exchange of a grass canopy. Remote Sens Environ. 1990;30:115–128.

25. Gilmanov TG, Tieszen LL, Wylie BK, Flanagan LB, Frank AB, Haferkamp MR, et al. Integration of CO_2 flux and remotely sensed data for primary production and ecosystem respiration analyses in the Northern Great Plains. Glob Ecol Biogeogr. 2005;14:271–292.

26. Prabhakara K, Hively WD, McCarty GW. Evaluating the relationship between biomass, percent groundcover and remote sensing indices across six winter cover crop fields in Maryland, United States. Int J Appl Earth Obs Geoinf. 2015;39:88–102.

27. Gitelson AA. Wide dynamic range vegetation index for remote quantification of biophysical characteristics of vegetation. J Plant Physiol. 2004;161(2):165–173.

28. CarbonTracker CT2019B [Internet]. Boulder (CO): National Oceanic and Atmospheric Administration; [cited 2026 Jan 10]. Available from: http://carbontracker.noaa.gov